DE GRUYTER OPEN

Preparation, structure and optical properties of transparent conducting gallium-doped zinc oxide thin films

J.H. Gu[1]*, Z. Lu[2], L. Long[2], Z.Y. Zhong[2,3], C.Y. Yang[2,3], J. Hou[2,3]

[1]Center of Experiment Teaching, South-Central University for Nationalities, Wuhan 430074, P. R. China

[2]College of Electronic Information Engineering, South-Central University for Nationalities, Wuhan 430074, P. R. China

[3]Laboratory of Intelligent Wireless Communications, South-Central University for Nationalities, Wuhan 430074, P. R. China

Highly conductive gallium-doped zinc oxide (GZO) transparent thin films were deposited on glass substrates by RF magnetron sputtering. The deposited films were characterized by X-ray diffraction (XRD), X-ray photoelectron spectroscopy (XPS), four-point probe and UV-Vis spectrophotometer, respectively. The effect of growth temperature on the structure and optoelectrical properties of the films was investigated. The results demonstrate that high quality GZO films oriented with their crystallographic c-axis perpendicular to the substrates are obtained. The structure and optoelectrical properties of the films are highly dependent on the growth temperature. It is found that with increasing growth temperature, the average visible transmittance of the deposited films is enhanced and the residual stress in the thin films is obviously relaxed. The GZO films deposited at the growth temperature of 400 °C, which have the largest grain size (74.3 nm), the lowest electrical resistivity (1.31×10^{-3} $\Omega \cdot$cm) and the maximum figure of merit (1.46×10^{-2} Ω^{-1}), exhibit the best optoelectrical properties. Furthermore, the optical properties of the deposited films were determined by the optical characterization methods and the optical energy-gaps were evaluated by extrapolation method. A blue shift of the optical energy gap is observed with an increase in the growth temperature.

Keywords: *zinc oxide; thin films; magnetron sputtering; optical properties*

1. Introduction

Gallium-doped zinc oxide (GZO) is a promising transparent conductive oxide (TCO) material for applications, such as transparent electrodes in photovoltaic solar cells [1–3], gas sensors [4], thin film transistors [5], liquid crystal displays [6] and organic light emitting devices [7, 8]. Besides high conductivity and optical transmittance in the visible region, the GZO thin films have a lot of advantages, such as low cost, non-toxicity, material abundance and high stability under hydrogen plasma, compared to ITO thin films. For the preparation of GZO thin films, there are many deposition techniques currently in use, for instance, RF magnetron sputtering [9–11], DC magnetron sputtering [12], spray pyrolysis [13], pulsed laser deposition [14], sol-gel process [15] and atomic

layer deposition [16]. Up to now, many research groups have reported the effect of deposition conditions on the properties of GZO thin films prepared by different methods. Gorrie et al. [9] studied the influence of deposition distance and temperature on electrical, optical and structural properties of RF magnetron-sputtered GZO thin films. They found that the changes in substrate temperature have a greater impact on the conductivity compared to changes in target-substrate distance. The highest conductivity (3200 S/cm) and mobility (20.7 cm^2/V·s) are obtained at the substrate temperature of 250 °C and at the target-substrate distance of 51 mm. Kim et al. [11] studied the dependence of resistivity and transmittance of RF sputter-deposited GZO thin films on substrate temperature and oxygen partial pressure. The transmittance of the GZO thin film is observed to be higher than 90 % in the visible range. The resistivity of GZO films decreases first and then increases

*E-mail: jhgalpha@163.com

as the substrate temperature increases from room temperature to 400 °C, and the minimum electrical resistivity of 3.3×10^{-4} Ω· cm can be obtained at 300 °C, while the resistivity hardly changes with the O_2/Ar flow ratio (R) for R < 0.25 but increases rapidly with R for R > 0.25. Bie et al. [12] studied the physical properties of GZO films prepared by DC reactive magnetron sputtering. They found that the substrate temperature have an important impact on the properties of GZO thin films. The thin film deposited at 350 °C exhibits relatively good crystallinity and the lowest electrical resistivity of 3.4×10^{-4} Ω·cm, while low-resistance and high transmittance GZO films can also be obtained at 150 °C by changing sputtering power. Gómez et al. [13] studied the effect of deposition temperature and dopant concentration [Ga/Zn] on the properties of GZO thin films obtained by chemical spray technique. The minimum electrical resistivity (7.4×10^{-3} Ω·cm) and the maximum figure of merit (5.1×10^{-4} Ω^{-1}) were obtained for the GZO thin films deposited at the substrate temperature of 425 °C using the solution with the [Ga/Zn] ratio of 2 at.%. In addition, Yamada et al. [17] reported that the lowest electrical resistivity of 2.1×10^{-4} Ω·cm can be achieved at the substrate temperature of 250 °C for the GZO thin films prepared by ion-plating method with DC arc discharge, while Nam et al. [16] found the lowest electrical resistivity to be about 1.5×10^{-3} Ω·cm for the GZO film grown at 300 °C by thermal atomic layer deposition. Furthermore, many authors adopted Taguchi method to investigate the effect of various deposition conditions on structure and optoelectronic properties of the GZO thin films, and found that the substrate temperature is one of the most important deposition parameters determining the film properties [18–20]. To our knowledge, although many experimental studies have been conducted on the synthesis, structural and optoelectrical properties of the GZO thin films, there are no detailed studies on optical constants and their dispersion behaviour, which are crucial to the structure design and performance improvement of optoelectronic devices. In this present work, transparent conducting GZO thin films were deposited on glass substrates by RF magnetron sputtering technique at different growth

temperatures. The structural, optical and electrical properties of the thin films were studied.

2. Experimental

2.1. Thin films preparation

Commercial plane glasses were cut into 30 mm × 30 mm plates and used as substrates in this experiment. Prior to their use, the glass substrates were successively washed in an ultrasonic bath of acetone, alcohol and deionized water, each for 15 min, and then dried in a high-purity nitrogen gas jet. The GZO transparent conducting films were deposited onto the previously cleaned glass substrates by RF magnetron sputtering system (KDJ-567) using a ZnO doped 3 wt.% Ga_2O_3 target (purity: 4N). Before deposition, the chamber was evacuated to an ultimate background pressure of 2.0×10^{-4} Pa using a turbo molecular pump. Then high-purity (99.99 %) argon gas was introduced into the chamber at a fixed flow rate of 20 sccm, and argon pressure was maintained at 0.5 Pa. Then, 10 min pre-sputtering, with the glass substrate covered by a closely mounted shutter, was employed to clean contamination on the target surface, followed by true sputtering. During deposition, the sputtering power was fixed at 180 W, and the target-substrate distance was kept at 75 mm. In order to investigate the effect of growth temperature (T_g) on properties of the films, the growth temperature T_g was varied from 50 °C to 500 °C.

2.2. Thin films characterization

The crystal structures of the deposited films were examined by X-ray diffraction (XRD, D8-ADVANCE) using standard CuKα radiation ($\lambda = 0.15406$ nm). The chemical states were analyzed by X-ray photoelectron spectroscopy (XPS, VG Multilab 2000) with monochromatic AlKα source under vacuum at 2.1×10^{-6} Pa. All of the binding energies were referenced to the C 1s peak at 284.6 eV of the surface adventitious carbon. The optical transmission spectra were recorded using a double beam UV-Vis spectrophotometer (TU-1901). The sheet resistance and electrical

resistivity were measured with a four-point probe measurement system (SZ-82).

3. Results and discussion

3.1. Structural properties

Fig. 1 presents the XRD patterns (θ to 2θ) of the GZO thin films deposited at different growth temperatures. For all the samples, the diffraction peak positions of 2θ located at about 31.1°, 34.2°, 55.3° and 62.2° are associated with the (100), (002), (110) and (103) planes of hexagonal phase according to the JCPDS Card No. 36-1451 (ZnO) [9, 21]. Obviously, the intensity of (002) peak is much stronger than that of the others. The result indicates that the GZO thin films have hexagonal wurtzite structure with highly c-axis orientation. Note also that neither metallic Zn or Ga characteristic peaks nor Ga_2O_3 phase is found from the XRD patterns, which implies that the Ga atoms either replace Zn atoms in the hexagonal lattice or segregate to the non-crystalline region in the grain boundary. Similar results for GZO thin films have been reported by many researchers [9, 13, 17]. The degree of preferred orientation of each film was estimated with the orientation factor $P_{(002)}$ [21, 22]:

$$P_{(002)} = \frac{I_{(002)}}{\sum I_{(hkl)}} \times 100\%, \qquad (1)$$

where $I_{(002)}$ is the (002) peak intensity, and $\sum I_{(hkl)}$ is the sum of the intensities of all the diffraction peaks for the GZO thin film. The value of $P_{(002)}$ is unity for a perfectly (002) oriented film. As shown in Fig. 1h, with increasing the growth temperature T_g from 50 °C to 400 °C, the $I_{(002)}$ and $P_{(002)}$ increase obviously, suggesting that the crystalline quality of the GZO thin films appears to become better, which is also reflected by the improvement of the electrical properties of the thin films. However, with the further increase from 400 °C to 500 °C, the $I_{(002)}$ and $P_{(002)}$ gradually decrease, the crystalline quality deteriorates. This result implies that the GZO thin films deposited at 400 °C exhibit the best crystal quality. At low growth temperature, the sputtered atoms possess less energy and low surface mobility. With the increase of the growth temperature, these atoms have sufficient energy

and surface mobility to settle in a stable position. This gives rise to the most stable c-axis oriented structure as preferred growth orientation. However, further increasing the growth temperature over 400 °C would lead to the increase of desorption rate for adsorption atoms resting on substrate surface. When the desorption rate is becoming greater than diffusion rate, large amounts of defects in films would produce, and then the crystalline quality of the deposited films become worse. Similar result has been reported previously by Cao et al. [23]. On the other hand, further increase of energy in the case of higher growth temperature over 400 °C could result in the breaking of the bonding of Zn–O and re-evaporation of the deposited films rather than enabling the atoms to move to their stable sites [12, 24], so as to decrease the orientation factor of (002) direction. Zhang et al. [25] and Zhong et al. [22] reported similar result in researching the influence of growth temperature on the structural properties of Al-doped ZnO thin films.

Fig. 2 displays the peak position (2θ) and full-width at half-maximum (FWHM, B) of (002) plane for the GZO films deposited at different growth temperatures. It is clear from Fig. 2a that the 2θ value continuously increases with the increment of growth temperature T_g. When the growth temperature is 450 °C, the value of 2θ is 34.403°, approaching the value (34.421°) of the undoped ZnO (JCPDS Card No. 36-1451). Note from Fig. 2b that the B value decreases significantly with the growth of temperature up to 400 °C, and then it increases slightly above 400 °C. From the values of 2θ and B of the (002) peak, the grain sizes (D) can be estimated by the Scherrer's formula [26, 27]:

$$D = \frac{K\lambda}{B\cos\theta}, \qquad (2)$$

where the constant K is the shape factor (K = 0.89), λ is the wavelength of X-rays used (λ = 0.15406 nm), B is the FWHM in radians and θ is the Bragg's diffraction angle [28]. The grain sizes D of the films deposited at different growth temperatures are plotted in Fig. 2c. The D values in the range of 8.0 nm to 74.3 nm are observed with the variation of the growth temperature from 50 °C
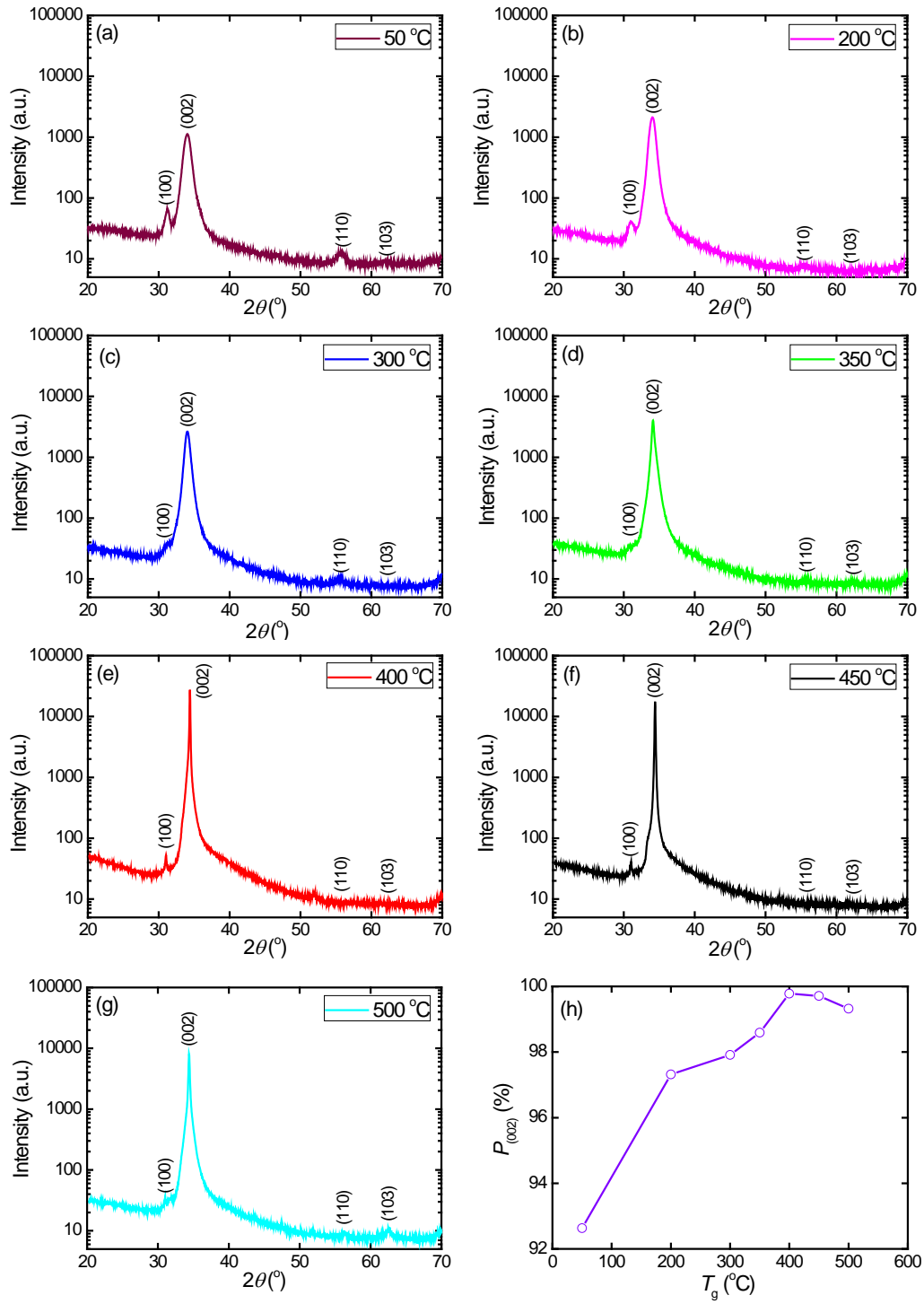
Fig. 1. XRD patterns of GZO films prepared at different growth temperatures (intensity axes are in logarithmic scale).

to 500 °C, and the maximum D value of 74.3 nm is obtained at the growth temperature of 400 °C.

The lattice constants of the deposited films were calculated from XRD data using the following equations [29–31]:

$$c = l \left[\frac{1}{d_{(hkl)}^2} - \frac{4(h^2 + k^2 + hk)}{3a^2} \right]^{-1/2} \quad (3)$$

$$d_{(hkl)} = \frac{\lambda}{2 \sin \theta} \quad (4)$$

where a and c are the lattice constants, the subscripts h, k and l are Miller indices, and $d_{(hkl)}$ is the crystalline plane distance for indices (hkl). According to equation 3, the lattice constant c is equal to 2d for the (002) diffraction peak. The residual stress (σ_{film}) in the plane of the film can be evaluated using the biaxial strain model [32, 33]:

$$\sigma_{film} = \left[C_{13} - \frac{C_{33}(C_{11} + C_{12})}{2C_{13}} \right] \frac{c - c_0}{c_0} \quad (5)$$

where C_{ij} are the elastic constants; the following values for single crystal ZnO are used [21, 34]: $C_{11} = 208.8$ GPa, $C_{12} = 119.7$ GPa, $C_{13} = 104.2$ GPa and $C_{33} = 213.8$ GPa. This yields the following numerical relation for the residual stress σ_{film} derived from the change in the 'c' lattice parameter:

$$\sigma_{film} = -232.8 \frac{c - c_0}{c_0} \text{ (GPa)} \quad (6)$$

where c is the lattice constant of the strained GZO thin films calculated from XRD result, and c_0 is the lattice constant of the undoped ZnO. Generally, the residual stress σ_{film} of a film deposited onto a substrate can be separated into two components [35]:

$$\sigma_{film} = \sigma_{th} + \sigma_{int} \quad (7)$$

where σ_{th} and σ_{int} are the intrinsic and thermal stresses, respectively. The thermal stress σ_{th} is given by the expression [36]:

$$\sigma_{th} = \frac{E_f}{1 - \nu_f} \Delta\alpha \cdot \Delta T \quad (8)$$

where E_f and ν_f are Young's modulus and Poisson's ratio of the thin film, respectively. $\Delta T = T_g - T_0$ is the temperature change, $\Delta\alpha = \alpha_f - \alpha_s$ is the difference in coefficients of thermal expansion between the thin film and the substrate. Using the values of $E_f = 123$ GPa, $\nu_f = 0.36$ and $\alpha_f = 5 \times 10^{-6}$ K^{-1} for GZO thin films and $\alpha_s = 9 \times 10^{-6}$ K^{-1} for the glass substrates [21, 36], the thermal stress σ_{th} at room temperature ($T_0 = 25$ °C) for the GZO samples deposited at different growth temperatures ($T_g = 50$ to 500 °C) were calculated by equation 8. After having obtained the residual stress σ_{film} and the thermal stress σ_{th}, the intrinsic stress σ_{int} of the deposited GZO films can be readily achieved using the relation (7). The stress results of the GZO thin films deposited at different growth temperatures are plotted in Fig. 2d. When the growth temperature varies from 50 °C to 350 °C, the negative sign of residual stress σ_{film}, intrinsic stress σ_{int} and thermal stress σ_{th} can be observed, indicating that the deposited films are in a state of compressive stress. Note also that the value of σ_{int} is much larger than that of σ_{th}. Thus, the residual stress σ_{film} might only be attributed to the intrinsic stress σ_{int}, rather than the thermal stress σ_{th}. On the other hand, the positive sign of respective values of σ_{int} can be remarked at the growth temperature larger than or equal to 400 °C. This means that the intrinsic stress σ_{int} is a tensile one. Hence, the contribution of intrinsic stress σ_{int} to the overall residual stress σ_{film} is to counteract the thermal stress σ_{th}. It is also found that the value of σ_{int} is slightly smaller than that of σ_{th}. The negative value of residual stress σ_{film} indicates that the thin films are in a state of compressive stress. The value of σ_{film} decreases significantly with the growth temperature up to 400 °C, and then it decreases slightly above 400 °C. The σ_{film} values are observed to be about 2.509 GPa, 2.092 GPa, 0.107 GPa and 0.106 GPa for the GZO thin films deposited at the growth temperatures of 300 °C, 350 °C, 400 °C and 450 °C, respectively. It indicates that the residual stress in the thin films is obviously relaxed with the increase of growth temperature, which is in good agreement with the results obtained by Kumar et al. [37] in ZnO film.
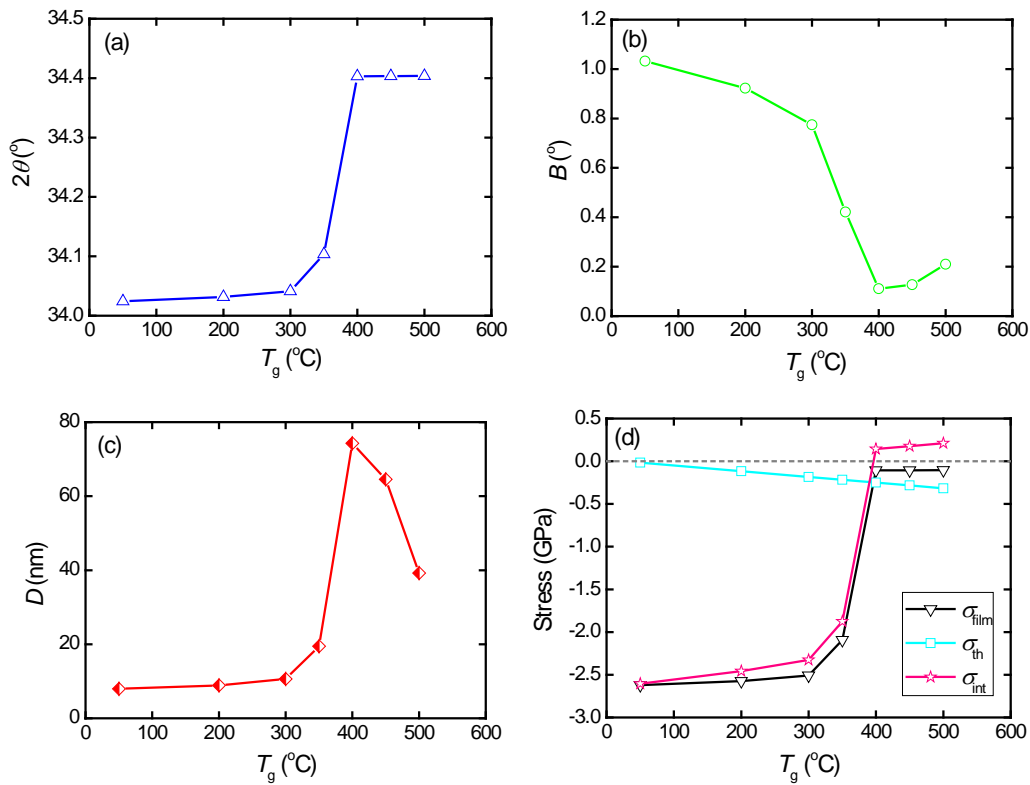
Fig. 2. The values of 2θ , B, D and σ for GZO films prepared at different growth temperatures.

Fig. 3a depicts the wide-scan XPS spectrum of the GZO thin films deposited at the growth temperature of 400 °C. In the XPS spectrum, the photoelectron peaks of Ga, C, O and Zn are detected, and the peaks located at about 20.3 eV, 530.4 eV, 1021.7 eV and 1044.8 eV correspond to Ga 3d, O 1s, Zn $2p_{3/2}$ and Zn $2p_{1/2}$, respectively. The peak centred at 284.6 eV corresponds to C 1s, suggesting that carbon is the only major contaminant. Similar results have also been reported previously by several groups [38–40]. Fig. 3b to Fig. 3d display the narrow-scan XPS spectra of Ga 3d, O 1s and Zn $2p_{3/2}$ for the sample. As can be seen, only a peak at 20.3 eV is detected in Ga 3d XPS spectrum, corresponding to Ga–O bond. It suggests that Ga is in its oxidization state and it is located at the Zn site in the GZO thin film, which is in agreement with the XRD measurements above. The O 1s peak can be fitted by two nearly Gaussian, centered at 530.1 eV and 531.2 eV, respectively. The peak located at lower energy (530.1 eV) accords

with Zn–O bond, while the higher energy peak (531.2 eV) accords with the chemisorbed oxygen [41]. Note that the core line of Zn $2p_{3/2}$ shows high symmetry and the binding energy of Zn $2p_{3/2}$ remains to be about 1021.7 eV, which confirms that the majority of Zn atoms remain in the same formal valence state of Zn^{2+} within the ZnO matrix [42]. In addition, no metallic Zn peak located at about 1021.5 eV [42] is observed in the XPS spectrum, indicating that Zn exists only in the oxidized state, which is consistent with the XRD analysis above.

3.2. Optical properties

Fig. 4 gives the optical transmission spectra of the GZO thin films deposited at different growth temperatures. The well oscillating transmittance curves can be observed for all the thin films, indicating low surface roughness and good homogeneity [43–45]. It is also found that the cut-off wavelength shifts towards the short side,
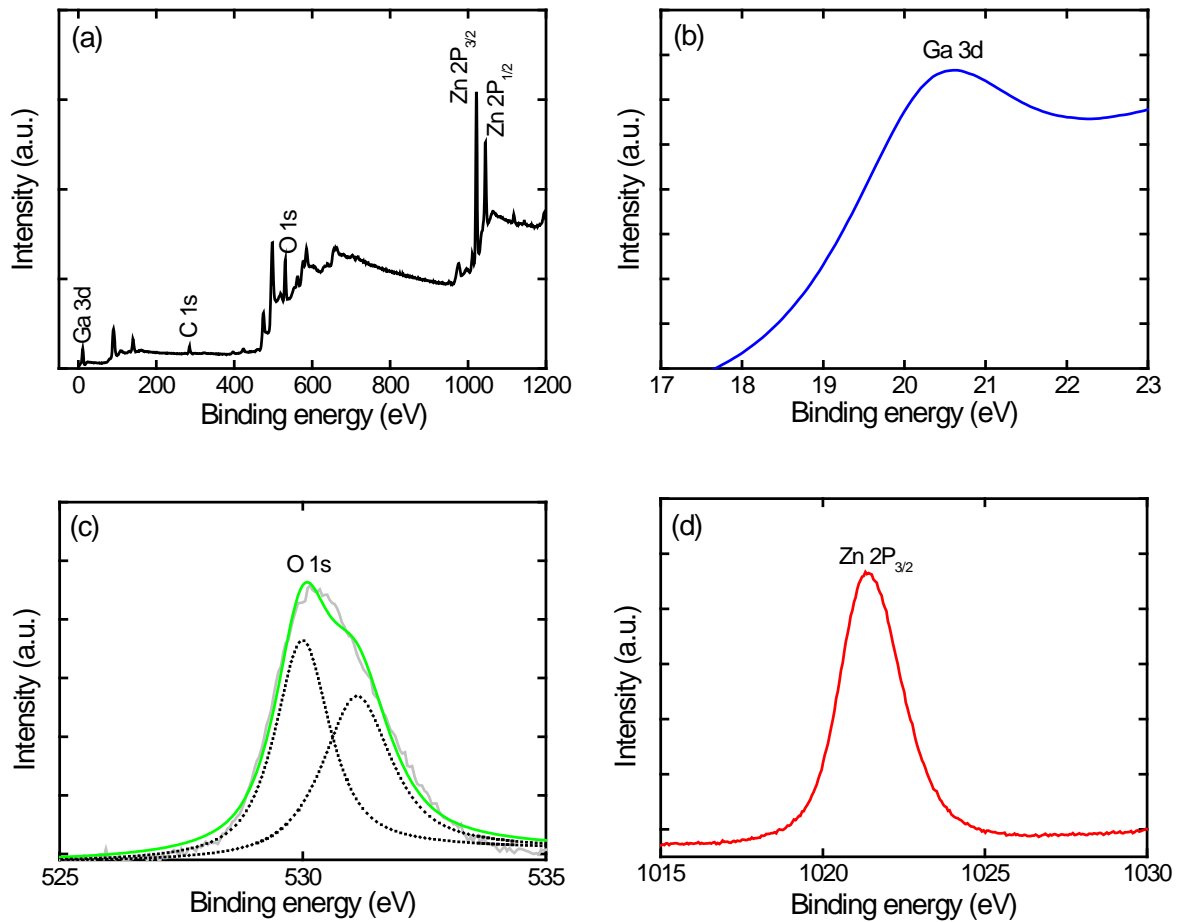
Fig. 3. The XPS spectra of the GZO films prepared at the growth temperature of 400 °C.

suggesting a widening of the optical energy-gap with increasing growth temperature. This blue-shift of the absorption edge can be explained by the Burstein-Moss effect in which the absorption edge shifts towards higher energy with an increase of carrier concentration. The average visible transmittance (T_{vis}) of all the thin films is plotted in the inset in Fig. 4. As can be seen, the average visible transmittance T_{vis} is over 83 % for all the deposited films, and the T_{vis} value monotonically increases with the growth temperature T_g.

From the measured transmittance spectra, the optical constants of the GZO thin films were determined using the method of optical spectrum fitting [46]. Fig. 5 shows the dependence of refractive index (n) and extinction coefficient (k) on wavelength (λ) for the thin films prepared at
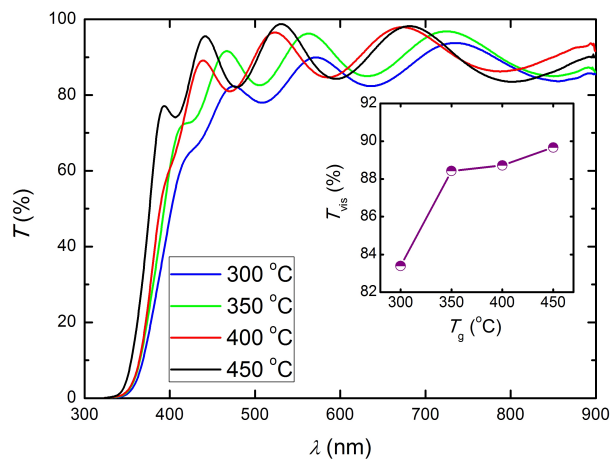

Fig. 4. Optical transmission spectra of GZO films prepared at different growth temperatures. The inset gives the average visible transmittance of all the films.

different growth temperatures. As can be seen, the extinction coefficient k of the thin films is very small in the visible region, indicating that the GZO thin films are highly transparent. The refractive index n is observed to decrease with increasing wavelength λ for the deposited films. When the growth temperature increases, the value of n increases initially and then decreases. At wavelength λ = 500 nm, corresponding to the growth temperatures of 300 °C, 350 °C, 400 °C and 450 °C, the values of n and k of the thin films are 2.075, 7.118×10^{-5}; 2.112, 2.755×10^{-7}; 2.251, 9.380×10^{-8}; and 2.184, 2.830×10^{-4}, respectively. The results in this present work are comparable to the results of previous studies. Wang et al. [47] reported that the n values of undoped ZnO thin films prepared by filtered cathode vacuum arc deposition, obtained by the envelope method, were 2.03 to 2.21 in the visible range, and the n values measured by spectroscopic ellipsometer by Hwang et al. [48], were about 1.93 to 2.18 in the visible range for Al-doped ZnO thin films deposited by reactive RF sputtering. Note also from Fig. 5 that the dispersion curve rises sharply towards shorter wavelength, displaying the typical shape of a dispersion curve near an electronic interband transition. The dispersion data of the n were analyzed by the Sellmeier's dispersion formula [49, 50]:

$$n^2 - 1 = \frac{E_d/E_o}{1 - \left(E/E_o\right)^2}, \qquad (9)$$

where E_d is the dispersion energy and E_o is the single-oscillator energy. The curves of $(n^2-1)^{-1}$ versus E^2 for all the thin films are plotted in Fig. 6 and the data are fitted into straight lines, indicating the Sellmeier's dispersion model is applicable to the GZO films in our work. The E_d and E_o values are deduced from the slope $(-1/E_dE_o)$ and intercept (E_o/E_d) on the vertical axis. The long wavelength refractive index (n_∞), the M_{-1} and M_{-3} moments of the optical spectra were calculated by the following formulae [51, 52]:

$$n_\infty = \left(1 + \frac{E_d}{E_o}\right)^{1/2}, \quad M_{-1} = \frac{E_d}{E_o}, \quad M_{-3} = \frac{E_d}{E_o^3}. \qquad (10)$$

The obtained results of n_∞, M_{-1} and M_{-3} are summarized in Table 1. The values of E_o can be observed to vary from 5.376 eV to 6.181 eV, and E_d from 14.707 eV to 20.190 eV for the films deposited at different growth temperatures T_g. Obviously, the E_o varies in a very narrow range compared with the E_d. Note also from Table 1 that all the parameters of the thin films are strongly dependent on the growth temperature.

Table 1. Optical properties of GZO films prepared at different growth temperatures.

T_g (°C)	E_o (eV)	E_d (eV)	n_∞	E_{-1}	E_{-3} (eV^{-2})
300	5.983	16.459	1.937	2.751	7.685×10^{-2}
350	5.376	14.707	1.933	2.736	9.466×10^{-2}
400	5.942	20.190	2.097	3.398	9.623×10^{-2}
450	6.181	19.762	2.049	3.197	8.369×10^{-2}

The optical energy-gap (E_g) of the thin films is determined by applying the Tauc model, and the Davis and Mott model in the high absorbance region [53, 54]:

$$(\alpha E)^m = A\left(E - E_g\right), \qquad (11)$$

where E is the photon energy, A is the constant, and α is the optical absorption coefficient. For m = 2 the transition data provide the best linear curve in the band-edge region, implying the transition is direct in nature. The energy-gap of the deposited films have been calculated using Tauc's plot by plotting $(\alpha E)^2$ versus E (Fig. 7) and by extrapolating the linear portion of the absorption edge to find the intercept with energy axis [55]. The dependence of optical energy-gap E_g on growth temperature T_g is shown in the inset of Fig. 7, and the E_g values of GZO thin films was calculated to be in the range of 3.385 eV to 3.511 eV. The GZO films in our study appear to have larger E_g compared to undoped ZnO films, due to the increase in carrier concentration caused by the contribution of Ga^{3+} ions at substitutional sites of Zn^{2+} ions and the higher energy-gap resulted from Ga interstitial atoms. Similar results have been reported previously by Chang et al. [56] and Gupta et al. [57] who studied the optical properties of Al-doped ZnO thin films and In-doped ZnO thin films.
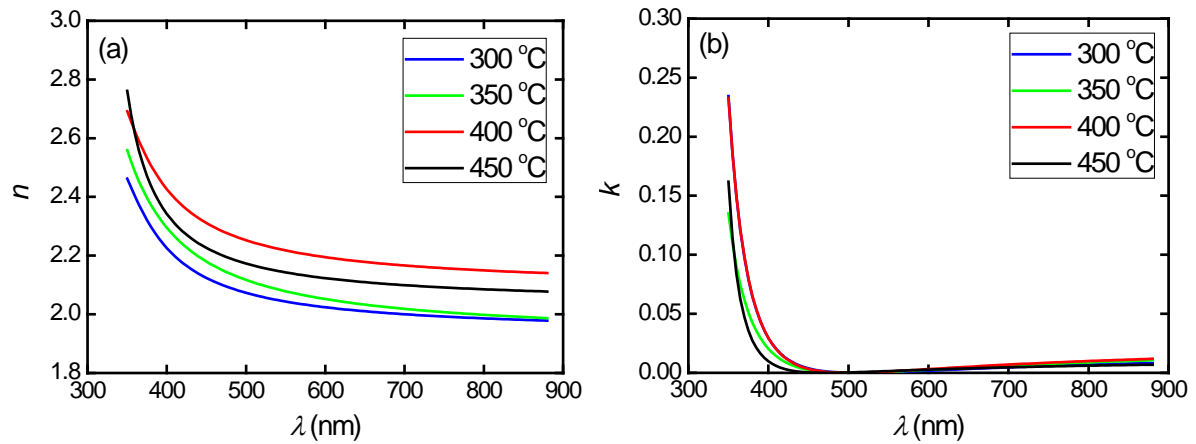
Fig. 5. The values of n and k for GZO films prepared at different growth temperatures.
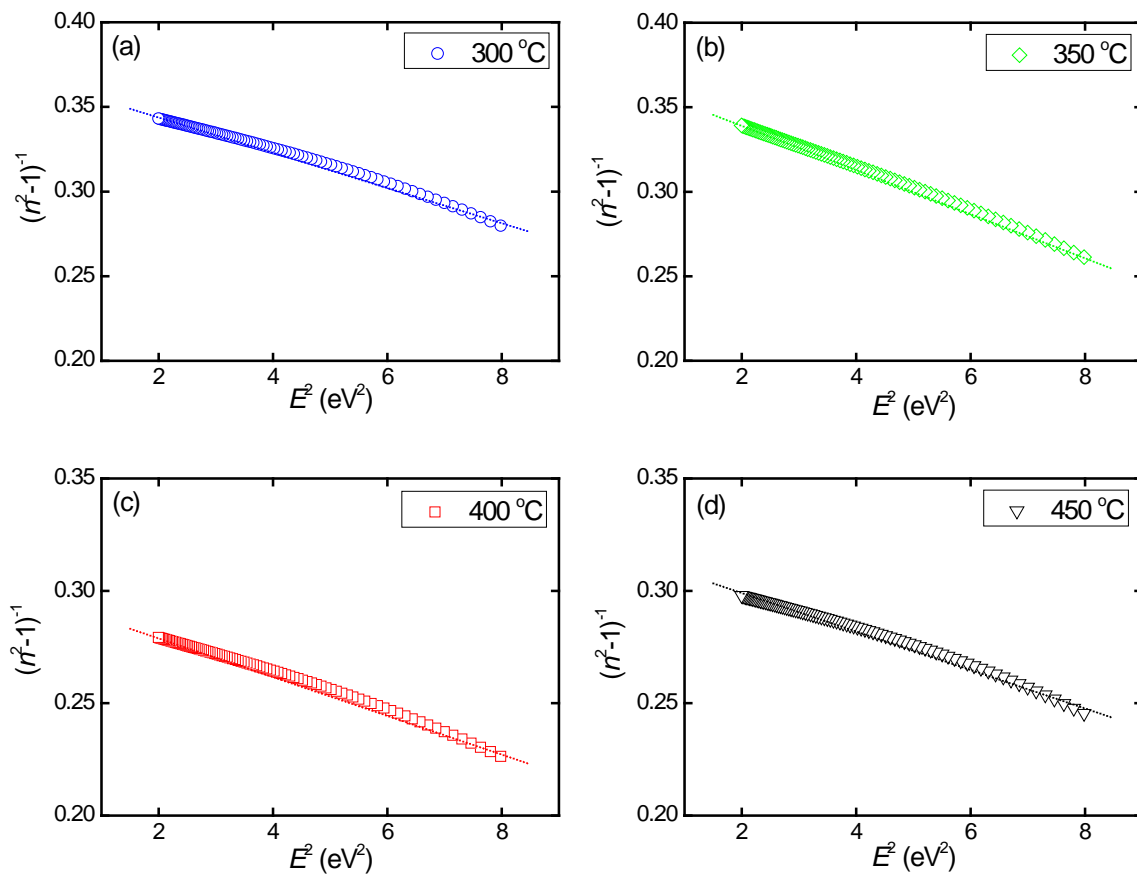

Fig. 6. The $(n^2 - 1)^{-1}$ versus E^2 plots of GZO films prepared at different growth temperatures.
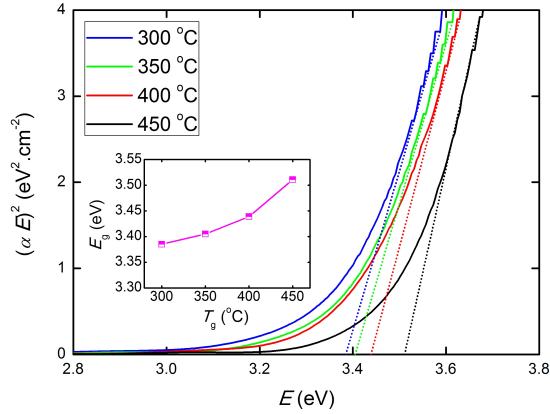
Fig. 7. The Tauc's plots of GZO films deposited at different growth temperatures. The inset shows the optical energy-gaps of all the films.
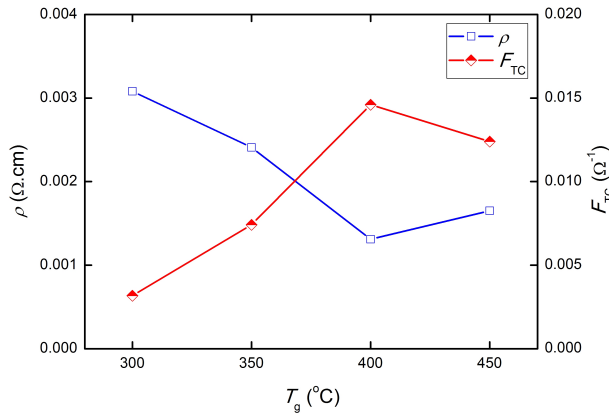

Fig. 8. The values of ρ and F_{TC} for GZO films deposited at different growth temperatures.

3.3. Electrical properties

Fig. 8 illuminates the electrical resistivity (ρ) of the GZO thin films deposited at different growth temperatures. As the growth temperature increases from 300 °C to 450 °C, the ρ first decreases and then increases. The lowest resistivity of 1.31×10^{-3} Ω·cm is obtained at the growth temperature of 400 °C. Similar variation tendency has been reported previously by Kim et al. [11]. The decrease in electrical resistivity can be attributed to the increase in grain size, which is confirmed by the results of XRD discussed above. The increase in the grain size can cause a decrease in grain-boundary scattering and an increase in carrier lifetime, and

consequently lead to an increase of both the carrier concentration and Hall mobility and, hence, result in a decrease in electrical resistivity [58, 59]. When the growth temperature increases from 300 °C to 400 °C, the grain size increases (from 10.6 nm to 74.3 nm) obviously, and the grain boundaries decrease rapidly, and thereby the electrical resistivity decreases sharply. With further increasing the growth temperature over 400 °C, however, the grain size decreases (from 74.3 nm to 64.6 nm) and the grain boundaries increase, and accordingly the electrical resistivity increases.

In order to quantify the optoelectrical properties of the deposited films, the figure of merit (F_{TC}) was calculated using Haacke's formula [60, 61]:

$$F_{TC} = \frac{T_{vis}^{10}}{R_{sh}}, \qquad (12)$$

where T_{vis} is the average visible transmittance and R_{sh} is the sheet resistance [62]. Fig. 8 shows the figure of merit (F_{TC}) as a function of growth temperature. As can be seen, the F_{TC} increases firstly and then decreases with the increment of the growth temperature. The best combination of high transmission and low resistivity, i.e. the maximal figure of merit $F_{TC} = 1.46 \times 10^{-2}$ Ω^{-1} is obtained at the growth temperature of 400 °C. Similar results, i.e. $F_{TC} = 0.13 - 1.50 \times 10^{-2}$ Ω^{-1} for typical Al-doped ZnO, GZO and ITO thin films, have been reported in the literature [63–65]. Obviously, the value of F_{TC} for the films grown at 400 °C is observed to be very close to the highest F_{TC} of the typical TCO candidate, indicating that the deposited thin films in our work have acceptable optical and electronic properties for potential applications as transparent conductive electrodes in photovoltaic solar cells, light emitting devices and flat panel displays.

4. Conclusions

In summary, transparent conductive GZO thin films were deposited on glass substrates by RF magnetron sputtering at different growth temperatures varying from 50 °C to 500 °C. The effect of growth temperature on the structural, optical and electrical properties of the thin films was

investigated. It is found that the growth temperature plays a prominent role on the structural, electrical properties of the films, but has not so much influence on the optical properties. The XRD patterns indicate that the deposited films are of c-axis preferred orientation. When the growth temperature is increased up to 400 °C, the crystallinity of thin films is improved, yet deteriorated at higher growth temperature over 400 °C. The residual stress in the deposited films can be observed to obviously relax with increase in growth temperature. The XPS spectra reveal that Ga atoms substitute Zn in the hexagonal lattice. Also, we can remark the presence of the chemisorbed oxygen in GZO thin films, while Zn as well as Ga exist only in oxidized state. Both the analyses of the XRD and XPS are consistent with each other. With the increment of growth temperature, the electrical resistivity of GZO films decreases first and then increases, but the average visible transmittance monotonically increases. The GZO thin film prepared at the growth temperature of 400 °C exbihits the lowest resistivity of 1.31×10^{-3} $\Omega \cdot$ cm and the highest figure of merit of 1.46×10^{-2} Ω^{-1} with the average visible transmittance of 89 %. Meanwhile, the optical constants were determined using the method of optical spectrum fitting from the measured transmittance spectra. The dispersion behavior of the refractive index was studied in terms of the Sellmeier's dispersion model, and the oscillator parameters of the thin films were achieved. Furthermore, the optical energy-gaps of the deposited films were calculated by extrapolation method from the Tauc's plots. The optical energy-gap of the thin films is observed to increase gradually from 3.385 eV to 3.511 eV with increasing the growth temperature. The results indicate that the control of growth temperature is an important factor in the fabrication of GZO transparent electrodes for optoelectronic devices.

Acknowledgements

References

[1] WONG L.M., CHIAM S.Y., HUANG J.Q., WANG S.J., CHIM W.K., PAN J.S., *Sol. Energ. Mat. Sol. C.*, 95 (2011), 2400.

[2] CHEN S.B., *J. South-Cent. Univ. Nationlities (Nat. Sci. Ed.)*, 33 (2014), 57.

[3] PARK H.-K., KANG J.-W., NA S.-I., KIM D.-Y., KIM H.-K., *Sol. Energ. Mat. Sol. C.*, 93 (2009), 1994.

[4] HU J., ZHOU Y., LIU H., MENG L., BAO M., SONG Z., *J. South-Cent. Univ. Nationlities (Nat. Sci. Ed.)*, 29 (2010), 6.

[5] LEE Y.-S., DAI Z.-M., LIN C.-I., LIN H.-C., *Ceram. Int.*, 38 (2012), S595.

[6] YAMAMOTO N., MAKINO H., OSONE S., UJIHARA A., ITO T., HOKARI H., MARUYAMA T., YAMAMOTO T., *Thin Solid Films*, 520 (2012), 4131.

[7] WAN L. SWENSEN G, J.S., POLIKARPOV E., MATSON D.W., BONHAM C.C., BENNETT W., GASPAR D.J., PADMAPERUMA A.B., *Org. Electron.*, 11 (2010), 1555.

[8] HE X., XIONG L., *J. South-Cent. Univ. Nationlities (Nat. Sci. Ed.)*, 30 (2011), 70.

[9] GORRIE C.W., SIGDEL A.K., BERRY J.J., REESE B.J., VAN HEST M.F.A.M., HOLLOWAY P.H., GINLEY D.S., PERKINS J.D., *Thin Solid Films*, 519 (2010), 190.

[10] ZHONG Z., ZHOU J., YANG L., *J. South-Cent. Univ. Nationlities (Nat. Sci. Ed.)*, 30 (2011), 34.

[11] KIM S., LEE W.I., LEE E.-H., HWANG S.K., LEE C., *J. Mater. Sci.*, 42 (2007), 4845.

[12] BIE X., LU J.G., GONG L., LIN L., ZHAO B.H., YE Z.Z., *Appl. Surf. Sci.*, 256 (2009), 289.

[13] GÓMEZ H., M. OLVERA DE LA L., *Mater. Sci. Eng. B-Adv.*, 134 (2006), 20.

[14] SANS J.A., SÁNCHEZ-ROYO J.F., SEGUR A A., *Superlattice. Microst.*, 43 (2008), 362.

[15] TSAY C.-Y., FAN K.-S., LEI C.-M., *J. Alloy. Compd.*, 512 (2012), 216.

[16] NAM T., LEE C.W., KIM H.J., KIM H., *Appl. Surf. Sci.*, 295 (2014), 260.

[17] YAMADA T., MIYAKE A., KISHIMOTO S., MAKINO H., YAMAMOTO N., YAMAMOTO T., *Surf. Coat. Tech.*, 202 (2007), 973.

[18] ZHU D.L., WANG Q., HAN S., CAO P.J., LIU W.J., JIA F., ZENG Y.X., MA X.C., LU Y.M., *Appl. Surf. Sci.*, 298 (2014), 208.

[19] CHU C.Y., HUANG C.H., KAO L.M., CHOU C.P., HSU C.Y., CHEN C.W., CHEN D.Y., *Superlattice. Microst.*, 49 (2011), 158.

[20] BIE X., LU J., WANG Y., GONG L., MA Q., YE Z., *Appl. Surf. Sci.*, 257 (2011) 6125.

[21] MALEK M.F., MAMAT M.H., MUSA M.Z., KHUSAIMI Z., SAHDAN M.Z., SURIANI A.B., ISHAK A., SAURDI I., RAHMAN S.A., RUSOP M., *J. Alloy. Compd.*, 610 (2014), 575.

[22] ZHONG Z., GU J., HE X., SUN F., *J. South-Cent. Univ. Nationlities (Nat. Sci. Ed.)*, 28 (2009), 33.

[23] Cao P.-J., Deng H.-F., Liu W.-J., Jia F., Zhu D.-L., Ma X.-C., Lv Y.-M., *Chin. J. Lumin.*, 33 (2012), 318.

[24] Kwak D.-J., Park K.-I., Kim B.-S., Lee S.-H., Lee S.-J., Lim D.-G., *J. Korean Phys. Soc.*, 45 (2004), 206.

[25] Zhang Z., Bao C., Yao W., Ma S., Zhang L., Hou S., *Superlattice. Microst.*, 49 (2011), 644.

[26] Sathyamoorthy R., Sharmila C., Natarajan K., Velumani S., *Mater. Charact.*, 58 (2007), 745.

[27] Chen D.H., Li Q.X., Huang J.P., *J. South-Cent. Univ. Nationlities (Nat. Sci. Ed.)*, 29 (2010), 14.

[28] Thanikaikarasan S., Mahalingam T., *J. Alloy. Compd.*, 511 (2012), 115.

[29] Fang G.J., Li D.J., Yao B.L., *Phys. Status Solidi A*, 193 (2002), 139.

[30] Chen S., Wei S., He X., Sun F., *J. South-Cent. Univ. Nationlities (Nat. Sci. Ed.)*, 31 (2012), 66.

[31] Cullity B.D., *Elements of X-ray Diffraction*, 2nd Ed., Addison-Wesley, Boston, 1978.

[32] Chen S.B., Sun F.L., *J. South-Cent. Univ. Nationlities (Nat. Sci. Ed.)*, 32 (2013), 59.

[33] Cebulla R., Wendt R., Ellmer K., *J. Appl. Phys.*, 83 (1998), 1087.

[34] Zhong Z., Gu J., He X., Sun F., Chen S., *J. South-Cent. Univ. Nationlities (Nat. Sci. Ed.)*, 30 (2011), 64.

[35] Liu J., Xia C., He X., Zhou G., Xu J., *J. Cryst. Growth*, 267 (2004), 161.

[36] Rusu G.G., Râmbu A.P., Buta V.E., Dobromir M., Luca D., Rusu M., *Mater. Chem. Phys.*, 123 (2010), 314.

[37] Kumar R., Khare N., Kumar V., Bhalla G.L., *Appl. Surf. Sci.*, 254 (2008), 6511.

[38] So S.K., Choi W.K., Cheng C.H., Leung L.M., Kwong C.F., *Appl. Phys. A-Mater.*, 68 (1999), 447.

[39] Li L., Fang L., Zhou X.J., Liu Z.Y., Zhao L., Jiang S., *J. Electron Spectrosc.*, 173 (2009), 7.

[40] Chen S.B, Wei S.L., He X, Sun F.L., *J. South-Cent. Univ. Nationlities (Nat. Sci. Ed.)*, 28 (2009), 43.

[41] Yen W.T., Lin Y.C., Yao P.C., Ke J.H., Chen Y.L., *Thin Solid Films*, 518 (2010), 3882.

[42] Yang W., Liu Z., Peng D.-L., Zhang F., Huang Y., Xie H., Wu Z., *Appl. Surf. Sci.*, 255 (2009), 5669.

[43] You Z.Z, Hua G.J., *Vacuum*, 83 (2009), 984.

[44] Zhong Z.Y., Zhang T., *Mater. Lett.*, 96 (2013), 237.

[45] Sun F., Hui S., *J. South-Cent. Univ. Nationlities (Nat. Sci. Ed.)*, 28 (2009), 10.

[46] Mulato M., Chambouleyron I., Birgin E.G., Martínez J.M., *Appl. Phys. Lett.*, 77 (2000), 2133.

[47] Wang M.-D., Zhu D.-Y., Liu Y., Zhang L., Zheng C.-X., He Z.-H., Chen D.-H., Wen L.-S., *Chin. Phys. Lett.*, 25 (2008), 743.

[48] Hwang Y.H., Kim H.M., Um Y.H., Park H.Y., *Mater. Res. Bull.*, 47 (2012), 2898.

[49] Aksoy S., Caglar Y., Ilican S., Caglar M., *J. Alloy. Compd.*, 512 (2012), 171.

[50] Zhong Z., Lan C., Wang H., *J. South-Cent. Univ. Nationlities (Nat. Sci. Ed.)*, 33 (2014), 51.

[51] El-Sayed S.M., *Vacuum*, 72 (2004), 169.

[52] Wemple S.H., Didomenico, JR, M., *Phys. Rev. B*, 3 (1971), 1338.

[53] Singh P., Kaushal A., Kaur D., *J. Alloy. Compd.*, 471 (2009), 11.

[54] Saravanan S., Anantharaman M.R., Venkatachalam S., Avasthi D.K., *Vacuum*, 82 (2008), 56.

[55] Gu J., Zhong Z., He X., Sun F., *J. South-Cent. Univ. Nationlities (Nat. Sci. Ed.)*, 28 (2009), 30.

[56] Chang J.F., Hon M.H., *Thin Solid Films*, 386 (2001), 79.

[57] Gupta R.K., Ghosh K., Patel R., Mishra S.R., Kahol P.K., *J. Cryst. Growth*, 210 (2008), 3019.

[58] Ma Q.-B., Ye Z.-Z., He H.-P., Zhu L.-P., Zhao B.-H., *Mat. Sci. Semicon. Proc.*, 10 (2007), 167.

[59] Lv M., Xiu X., Pang Z., Dai Y., Han S., *Appl. Surf. Sci.*, 252 (2005), 2006.

[60] Kim D.-K., Kim H.-B., *J. Alloy. Compd.*, 522 (2012), 69.

[61] Haacke G., *J. Appl. Phys.*, 47 (1976), 4086.

[62] Zhong Z., Zhang T., Wang H., *J. South-Cent. Univ. Nationlities (Nat. Sci. Ed.)*, 32 (2013), 58.

[63] Gontijo L.C., Machado R., Nascimento V.P., *Mater. Sci. Eng. B-Adv.*, 177 (2012) 780.

[64] Kim C.E., Moon P., Yun I., Kim S., Myoung J.-M., Jang H. W., Bang J., *Expert Syst. Appl.*, 38 (2011) 2823.

[65] Zhang B., Dong X., Xu X., Wang X., Wu J., *Mat. Sci. Semicon. Proc.*, 10 (2007) 264.